Applied Energy 343 (2023) 121055

Contents lists available at ScienceDirect

Applied Energy

journal homepage: www.elsevier.com/locate/apenergy

An investigation on plant cell walls during biomass pyrolysis: A histochemical perspective on engineering applications☆

Yoong Xin Pang [a], Nusrat Sharmin [b], Tao Wu [c,d], Cheng Heng Pang [a,d,e,*]

[a] Department of Chemical and Environmental Engineering, The University of Nottingham Ningbo China, Ningbo 315100, PR China
[b] Nofima Norwegian Institute of Food, Fisheries and Aquaculture Research, Tromsø, Norway
[c] New Materials Institute, The University of Nottingham Ningbo China, Ningbo 315100, PR China
[d] Key Laboratory for Carbonaceous Wastes Processing and Process Intensification Research of Zhejiang Province, University of Nottingham Ningbo China, Ningbo, 315100, PR China
[e] Municipal Key Laboratory of Clean Energy Conversion Technologies, University of Nottingham Ningbo China, Ningbo 315100, China

HIGHLIGHTS

- Fast green mainly stains primary cell walls that largely contain cellulose.
- Safranin O has greater affinity to lignified secondary cell walls.
- Biomass cells decompose into bio-char in three graphitisation stages.
- Primary cell walls are generally devolatilised and produce brittle bio-char.
- Secondary cell walls transform into thick and crystalline bio-char structures.

GRAPHICAL ABSTRACT

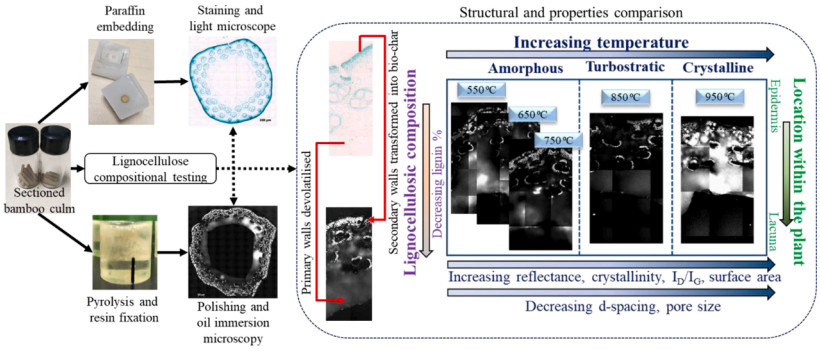

ARTICLE INFO

Keywords:
Lignocellulose
Image analysis
Pyrolytic products
Safranin O/fast green
Microscopy

ABSTRACT

The large variation in biomass species, and hence lignocellulosic composition, often results in varying properties and production of pyrolytic products, i.e. bio-char, bio-oil and bio-gas. Hence, understanding of the distribution of individual lignocellulosic components in plant cell walls and its influence on cell structural evolution during pyrolysis is essential to predict biomass behaviour for different engineering applications. Bamboo shoot sections were subjected to histochemical safranin O/fast green solution staining to reveal the distribution of lignocellulosic components in the sample. Stained fresh samples were compared against pyrolysed samples under light and oil immersion microscopy to investigate the structural evolution of primary and secondary cell walls during pyrolysis. Charred samples were subsequently characterised via BET, XRD and Raman spectroscopy to further understand the influence of pyrolytic temperatures on cell transformations. This study provides insights into understanding the devolatilisation and graphitisation characteristics of individual plant cell wall and its

☆ The short version of the paper was presented at CEN2022, April 23–25, 2022. This paper is a substantial extension of the short version of the conference paper.

* Corresponding author at: Department of Chemical and Environmental Engineering, The University of Nottingham Ningbo China, Ningbo 315100, PR China.
E-mail address: chengheng.pang@nottingham.edu.cn (C.H. Pang).

https://doi.org/10.1016/j.apenergy.2023.121055
Received 2 December 2022; Received in revised form 9 March 2023; Accepted 25 March 2023
Available online 11 May 2023

lignocellulosic components, thus facilitating biomass selection for targeted applications in energy derivation and/or material engineering without the need of repeating chemical-intensive histochemical and pyrolysis procedures.

1. Introduction

As the world faces the increasing challenge of resource depletion, renewable biomass has been exploited as a sustainable alternative source [1] to reduce the dependency on fossil resources for various applications. Biomass refers to organic materials derived from living organisms [2] and contains cellulose (C), hemicellulose (H), and lignin (L) as the three main components that make up 90 wt% of plant cell dry weight [3], with the remaining fractions of phenolic substitutes, protein, lipid, starch, and ash. C, H and L deposit into primary and secondary cells according to biological functions and cell growth processes. Primary walls consist of cellulose embedded in different types of hemicelluloses and pectin substrates [4], and will retain without major structural change after plant growth seize. Secondary cell walls are more common to expand as new layers during lignin deposition within the existing walls, which ultimately provide additional support and rigidity to the plant [5].

Biomass is conventionally processed via the most established pyrolysis technology [6] where the organic constituents in biomass decompose in a non-oxidative environment, yielding bio-char, bio-oil and biogas. The primary applications of both bio-oil and bio-gas are for heat and power generation [7]. Conversely, bio-char as the main solid product containing carbon residues is generally applied in soil and waste management [8] and has recently progressed into material sciences where the highly porous carbon-based bio-char is a potential precursor for the fabrication of advanced materials, in particular, nanomaterials [9]. However, the inconsistency in intrinsic properties and complex C, H and L compositions of biomass results in unpredictable processing and subsequently impacts the end products and their potential applications. Hence, it is crucial to understand the decomposition behaviour of individual components in biomass, and the influence of pyrolytic conditions on respective degradation.

The kinetic studies of biomass pyrolysis are initially performed via experimental approaches including thermogravimetric analysis [12], thermal analysis–mass spectrometry (TA–MS) [10], and synchrotron vacuum ultraviolet photoionisation mass spectrometry (PIMS) [11]. These approaches developed mechanistic kinetic models to understand molecular reactions and to predict major components in product yield. However, experimental techniques often encounter challenges such as losing track of particle residence time, difficulty in closing the mass balance and limited coverage of temperature range, during the derivation of accurate kinetics [12]. Hence, researchers employed various computational fluid dynamic (CFD) models and dynamic process simulations to further examine the biomass reaction mechanisms. CFD model developed with first-order single-step mechanisms [13] has detailed the devolatilisation of cacao shells at low and high temperature regimes whilst a CFD model developed for laminar entrained flow reactor has simulated full-scale processing with improved energy balance and accuracy of the similar studies [14]. In addition, computational models from Aspen Plus®, Matlab® and Intelligen SuperPro Designer were also built to simulate the actual kinetic decomposition paths of lignocellulose [15,16]. The product yield and distribution were reported to be highly influenced by C, H and L compositions [17].

Despite various efforts to investigate the stoichiometries of the global biomass pyrolysis reactions, identifying C, H and L distribution in plants is equally crucial to understand the cross-linking chemistry and polymeric architecture of biomass so as to maximise the potential of biomass samples targeted for specific applications. However, the actual structural transformations of biomass cells and lignocellulosic components during pyrolysis are yet to be discussed. Therefore, this study aims to (1) understand the anatomy of biomass cells and the distribution of lignocellulosic components in such cells; (2) identify the structural evolution of biomass cells during pyrolysis; (3) understand the influences of pyrolytic conditions on the final pyrolytic product distribution, bio-char structure and properties. Specifically, this work incorporates histochemical approaches to visualise the distribution of C, H and L in different biomass cells, and by coupling with the oil immersion microscopic view of pyrolysed samples, both techniques provide a clear comparison of the structural change of original biomass and final bio-char product. Additional characterisations of bio-char are performed to further quantify the quality of the bio-char. In general, this study provides insights into biomass behaviour during pyrolysis, thus expanding the potential of biomass utilisation in energy and material discovery sectors via efficient and effective selection based on the compositions of C, H and L and/or the different cell types in biomass.

2. Methodology

Bamboo shoot was harvested from an agricultural farm in Henan, China. Fresh culm was cut into identical 2 cm sections and subjected to: (1) histochemical staining to identify the primary and secondary walls via the distribution of lignocellulosic components across the sample; (2) compositional analysis for the quantification of cellulose (C), hemicellulose (H) and lignin (L) percentage in the sample; and (3) pyrolysis to obtain charred sections. Microscopic views and characterisations of both stained and charred sections were analysed and discussed.

2.1. Histochemical staining

Cross sections of bamboo at 2 cm were cut and fixed in FAA solution (50 mL of 40% formaldehyde, 50 mL of glacial acetic acid and 90 mL of 50% ethanol) for 24 h. The samples were softened and dehydrated at 55 °C, followed by paraffin embedding and cooling at −20 °C. Embedded shoots were sliced on a sliding microtome into 2 μm thick cross sections and subjected to histochemical staining. Successive sections were divided into three groups where group 1 sample was stained with safranin O solution for 2 h whilst group 2 sample was stained with fast green solution for 15 s. Group 3 sample was immersed in safranin O solution for 2 h, rinsed with ethanol for 5 s and counterstained with fast green solution for 15 s. All sample slides were rinsed with ethanol for 5 s after staining and mounted with resin and coverslip ready for observation.

2.2. Biomass compositional analysis

Bamboo culms from the same shoot were subjected to proximate analysis in accordance with the standard ASTM E1131 where bamboo sample was heated from room temperature to 900 °C under nitrogen flow of 50 mL/min and was combusted at 900–1000 °C for ash content evaluation. Similarly, the bamboo culms were also sectioned into 2 cm for lignocellulosic compositional analysis via the gravimetric method [18]. Air-dried sections were weighed and boiled in 2:1 ethanol-acetone for 4 h in a Soxhlet extractor, rinsed thoroughly with distilled water and dried at 105 °C for 24 h. The dried samples were divided into two equal parts in which one was identified as fraction A and the other, fraction A' was treated with 24% potassium hydroxide (KOH) for 4 h at 25 °C, washed thoroughly and dried at 80 °C for 24 h. After treatment, the dry weight of fraction A' was taken as fraction B. Fraction B was then hydrolysed with 72% sulphuric acid (H_2SO_4) for 3 h at room temperature, rinsed and further refluxed with 5% H_2SO_4 at 90 °C for 2 h. The

mixture was filtered, washed thoroughly with distilled water and oven-dried at 80 °C for 24 h. The dried fraction was weighed and recorded as fraction C. Cellulose, hemicellulose and lignin content in the bamboo samples were calculated based on equations (1) to (3).

Cellulose = (B – C) (1)

Hemicellulose = (A – B) (2)

Lignin = C (3)

2.3. Biomass pyrolysis

Bamboo culms of 2 cm were dried at 105 °C for 24 h to ensure maximum moisture removal. The dried sample was heated in a vertical quartz tube furnace (MTI-Corporation OTF-1200X) over a temperature range of 550–950 °C at a heating rate of 5 °C min^{-1}. Constant nitrogen atmosphere was maintained throughout the process by supplying N_2 gas at a flow rate of 120 mL min^{-1}. A condenser was connected to collect the condensables whilst a gas bag was used to collect non-condensable volatiles. The remaining solids in the tube furnace are bio-char. The schematic diagram of biomass pyrolysis is illustrated in Fig. 1. The pyrolytic product yields were expressed as weight percentage of the total mass of biomass sample used in each experiment as described in equation (4).

$$\text{Yield} = \frac{\text{Mass of pyrolytic product (g)}}{\text{Mass of biomass (g)}} \quad (4)$$

2.4. Microscopy and MosaicX imaging

Histochemical sample slides were observed under brightfield transmitted light microscope whilst charred bamboo samples were carefully fixed in 1:2.5 of EpoThin® Epoxy resin-hardener, polished with Eco-Met™ 250 Grinder Polisher before observing under the oil immersion objective. Images for both stained and charred samples were captured by using the MosaicX imaging function of Carl Zeiss Axio Imager. Mosaic tile sizes of 175.71 × 131.65 μm were captured to resemble the full cross sections of bamboo sections under 500X magnification.

2.5. Bio-char characterisations

The surface area and pore parameters of bio-char were analysed by using the automated nitrogen multilayer absorption system of Micromeritics ASAP 2010. The bio-char samples were first degassed at 120 °C for 14 h, followed by absorption and desorption over a relative pressure range of 0.001–0.995. Raman spectra were performed on Britain Renishaw RM2000 with a 514 nm laser source for a spectrum range of 300–4000 cm^{-1}. BRUKER D8 Advance X-Ray Diffraction apparatus (Cu Kα copper radiation of λ = 0.15405 nm, 40 kV and 40 mA) was used to determine the crystallinity and crystallographic structure of the produced bamboo char samples. The samples were scanned with a scan speed of 0.02°/s over a range of 10–90°. The lattice parameters of bio-char samples are calculated based on the Bragg's and Scherrer empirical equations (Eqs. (5)–(7)) [19,20].

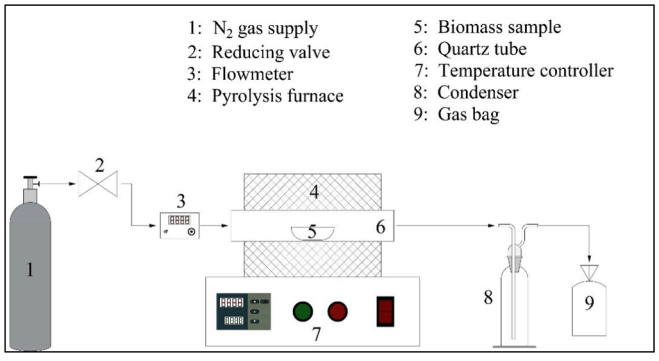

Fig. 1. Schematic drawing of biomass pyrolysis.

$$d = \frac{\lambda}{2\sin\theta} \quad (5)$$

$$Lc = \frac{k_c\lambda}{\beta_{002}\cos\theta_{002}} \quad (6)$$

$$La = \frac{k_a\lambda}{\beta_{100}\cos\theta_{100}} \quad (7)$$

The crystallite lattice parameters evaluate the interlayer spacing of aromatic layers (d), crystallite height (L_c) and crystallite diameter (L_a) where λ is the X-ray wavelength (1.5406 A); Θ_{002}, Θ_{100} and β_{002}, β_{100} are the peak positions (°) and full width at half-maximum (FWHM) (°) of (0 0 2) and (1 0 0) bands, respectively; k_c and k_a are constants of the X-ray reflection plane where (0 0 2) band takes the value of 0.89 whilst (1 0 0) band takes the value of 1.84.

3. Results and discussion

Amongst various biomass categories, Plantae kingdom is the dominant class of biomass accounting for 82% of the global biomass resource [21]; and C, H and L are the three main components that make up 90 wt % of most plant cell dry weight. Typically, lignocellulosic biomass contains 30–50 wt% of cellulose, 10–40 wt% of hemicellulose and 5 to 30 wt% of lignin [22]. Hence, the focused study on these fundamental constituents can be considered representative of the majority of lignocellulosic samples.

In addition, the selection of bamboo as the targeted sample in this study is inspired by a developed Piper diagram that considers technical, economical and environmental aspects during biomass processing [22]. Given that microcrystalline structures unique to cellulose may contribute to the production of crystalline bio-char in pyrolysis and cellulose (the most abundant constituent in biomass) is embedded within lignin, the selected bamboo sample with the sum of cellulose and lignin content >70%, could effectively reflect the bio-char structural transformation during pyrolysis. Moreover, owing to the abundance and accessibility of bamboo in the aspect of land occupancy and production mass, i.e., 6.67 million hectares of bamboo forest distributed across 21 provinces [23] and yields an annual 7 million tonnes of harvest [24] in Mainland of China, bamboo is selected to be used in this study.

3.1. Histochemical staining of biomass lignocellulosic components

Histochemical techniques have been applied to investigate the presence and distribution of lignocellulosic components in biomass tissues. Successful staining is a three-dimensional phenomenon dependent on both the chemical and physical aspects of dye sorption. Amongst the many staining techniques, safranin O, a cationic dye, generally has a preferential affinity for lignin. The charge-staining phenomena occur when the acidic and negatively charged groups in lignin are activated by wet mount during preparation procedures. On the contrary, preferential dye adsorption onto cellulose is associated with the neutral cellular macromolecules and domains. The fast green solution, a direct dye for cellulose staining typically contains anionic groups which would not be electrostatically repelled by the uncharged cellulose polymers. The uptake of cellulose dye is highly dependent on the cellulose pore size, directionality and orientation of cellulose crystals in natural fibres. Natural cellulose in plants exhibit heterogeneity, i.e., both hydrophobicity and hydrophilicity, depending on binding modules and crystal surfaces [25,26]. Research reports that the 110 crystal face of cellulose exhibits higher hydrophobicity [27] than other cellulosic components,

thus facilitating the uptake of hydrophobic fast green solution.

Safranin O is counterstained with fast green solution to identify cellulose and lignin contents in biomass. Counterstaining is based on a principle where a first dye stained on wood tissues is partially removed and replaced by a second dye to create better contrast for observations. Fast green solution shows a high affinity for cellulose whilst counterstaining of safranin produces a gradient from pink to red, with darker staining corresponding to the lignified vessel walls.

The bamboo section has a higher affinity for fast green staining as illustrated in Fig. 2a, particularly at the periphery of the sample, as compared to the intensity of safranin O staining as illustrated in Fig. 2b. During the cross-staining of sample as illustrated in Fig. 2c, the contrasting effect of both the dyes is less apparent where the red safranin dye is less visible in the section. The aforementioned phenomena indicated that the sample has higher cellulose content as compared to lignin, which is also evident and apparent from the lignocellulosic composition analysis of bamboo sample as tabulated in Table 1. In addition to that, proximate analysis indicated that bamboo sample contained mainly organic constituents with minor fraction of inorganic ash components, hence, subsequent analyses focus on the behaviour of organic matters in plant during pyrolysis.

Dermal, vascular and ground tissues as illustrated in Fig. 2d and 2 g are the three main plant tissue types developed through primary and secondary growth. The primary walls are gel-like composites comprised of cellulose, hemicellulose, proteins and a small amount of phenolic acids at the early stage of plant growth. Deposition of lignin occurs in secondary cell walls for mechanical support at maturity. These tissues are formed from complex organic composites and are specialised cells that fulfil specific functions in the lifecycle. The dermal tissues in bamboo stems are waxy cuticles that prevent excessive evaporation or

Table 1
Proximate analysis and lignocellulosic compositions of bamboo sample.

Components	Distribution (%)
Proximate analysis (wt% on dry basis)	
Moisture	7.0
Volatiles	76.0
Fixed carbon	9.0
Ash	8.0
Lignocellulosic compositions (%)	
Cellulose	60.3
Hemicellulose	13.8
Lignin	13.2
Others	12.7

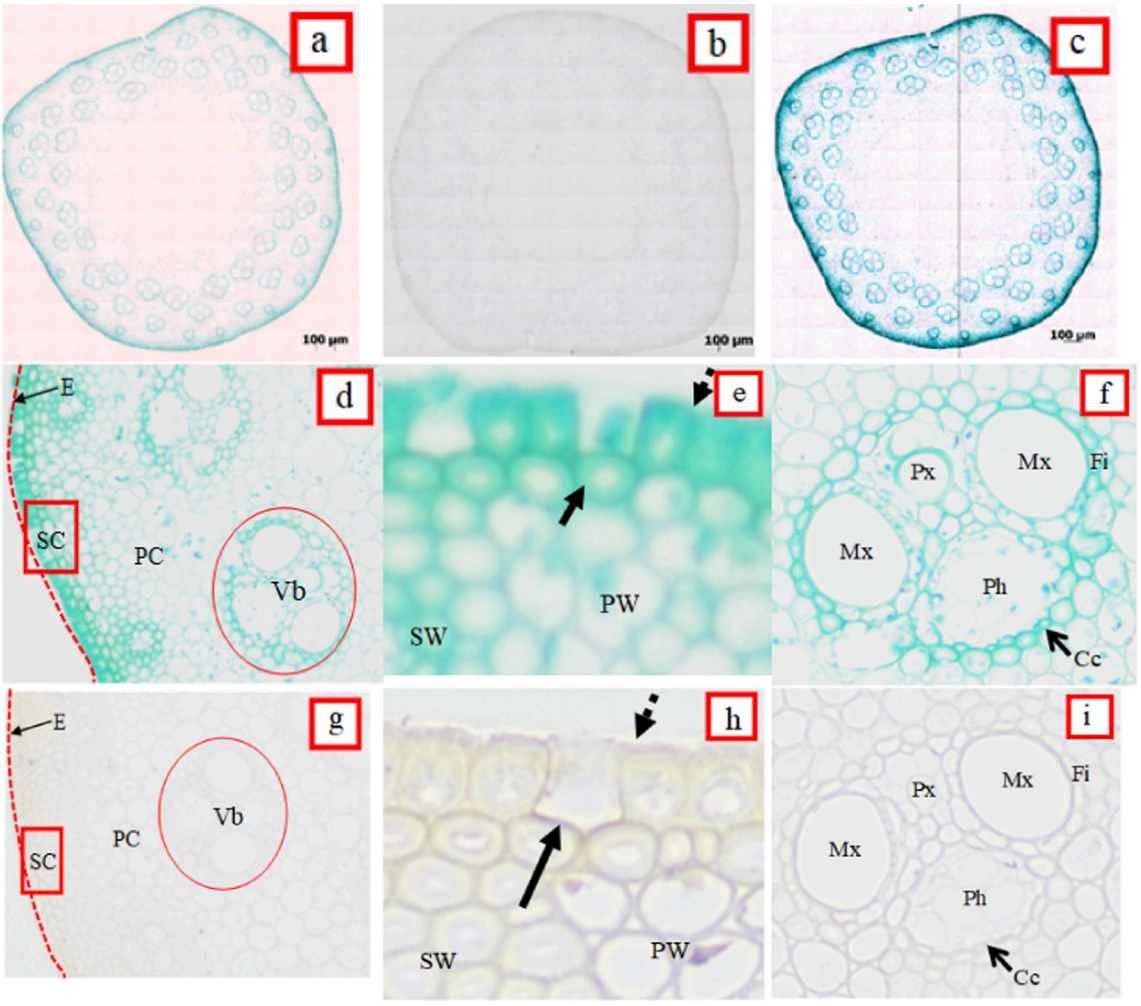

Fig. 2. Histochemical staining of bamboo cross section by using (a) fast green; (b) safranin O; and (c) safranin O fast green solution. (d) and (g) Overview of a bamboo culm cross section stained with fast green and safranin O solution, respectively where E: epidermis, SC: sclerenchyma cells, PC: parenchyma cells, and Vb: vascular bundle. (e) and (h) Cross section of sclerenchymatous layer accompanied by some parenchyma cells beneath the epidermis (dotted arrow), along with cellulosic G-layer (short solid arrow) and lignified middle lamella (long solid arrow) where SW: secondary walls, and PW: primary walls. (f) and (g) Cross section of vascular bundle where Mx: metaxylems; Px: protoxylem; Ph: phloem; Fi: fibre sheath and Cc: companion cells.

water loss. Beneath the epidermis, thick-walled and lignified sclerenchymatous cells, as illustrated in Fig. 2e and 2 h, are developed, followed by the cortex where the size of thin-walled and unlignified parenchyma cells gradually increase in size across the culm towards lacuna, the central cavity.

Bamboo culms generally consist of approximately 50% parenchyma, 40% sclerenchyma fibres and 8% vascular bundles. As apparent in Fig. 2e and 2 h, the lignified middle lamella (reddish-purple) is sharply differentiated from the unlignified primary walls (slight tinge of pink) whilst the gelatinous layers (G-layers) with cellulosic nature are highly stained by fast green solution, indicating a higher percentage of cellulose in between the G-layers.

The vascular bundles of bamboo consist of two metaxylem vessels, an elongated-oval phloem and a protoxylem as illustrated in Fig. 2f and 2i. The protoxylem, with a relatively smaller intercellular space as compared to metaxylem, is considered as a special feature in the culm structure as the intercellular layers undergo annual thickening without involving lignified cells. The intervening wall areas remain parenchymatous and are rigid and flexible to control the water flow across the stem. Fig. 2f reveals the staining of fast green solution with a denser contrast whilst protoxylem in Fig. 2i is stained with minimum, or none safranin O solution, indicating a higher cellulose content in the protoxylem. On the contrary, metaxylems are large vessels separated by lignified sclerenchyma cells consisting of primary and secondary walls. Both Fig. 2f and 2i reveal fibre sheath structures surrounding the metaxylems. As a characteristic feature, the fibre sheaths around vascular bundles are sickle-shaped sclerenchymatous tissues that are smaller in size than those beneath the epidermis.

As similar to parenchyma, vascular bundles exhibit different appearances across the culm where the bundles nearer to the periphery are smaller and the xylem fibre sheaths are often amalgamated into an ellipsoid, thus xylem sheaths appear to be larger than phloem sheaths. Conversely, vascular bundles nearer to the lacuna have individual strands isolating phloem and xylems, and are often observed with the existence of companion cells.

3.2. Influences of pyrolysis conditions

3.2.1. Lignocellulose degradation path

The degradation paths of biomass during pyrolysis are investigated based on a multistep reaction model describing the reactions in three main stages, namely (1) the releasing of free moisture, (2) primary decomposition into permanent gas, condensable vapour and solid residue, and (3) secondary cracking and repolymerisation. It is acknowledged that all three lignocellulosic components contribute to the formation of bio-oil, bio-gas and bio-char. However, due to their inherent nature, cellulose, hemicellulose and lignin undergo distinctive decomposition paths and hence, yield different weight percentages of pyrolytic products. The detailed kinetic rates and degradation paths have been reported and validated in previous work [17], concluding

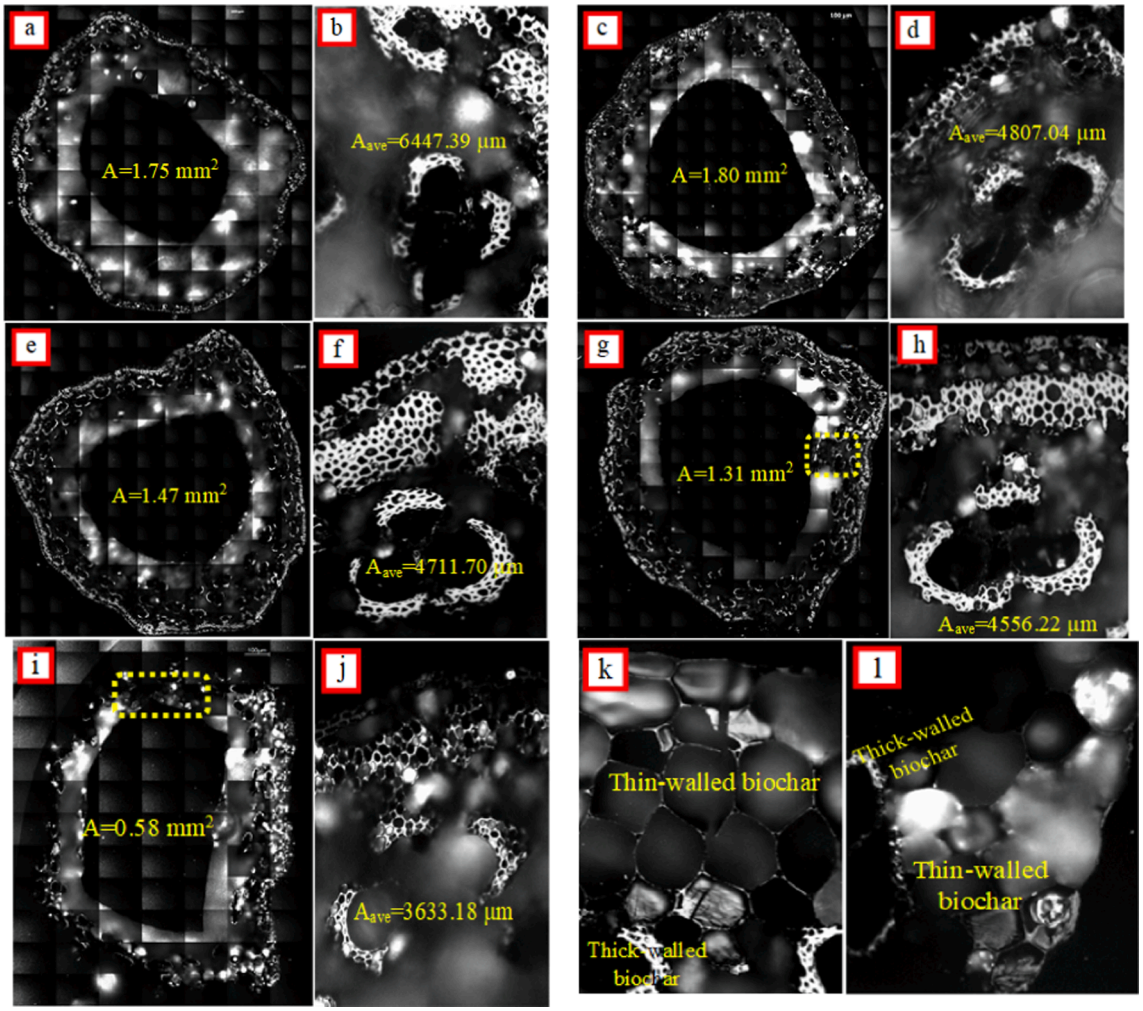

Fig. 3. Full cross-section of bamboo samples paired with focused sclerenchymatous layer and vascular bundle pyrolysed at a temperature of (a-b) 550, (c-d) 650, (e-f) 750, (g-h) 850 and (i-j) 950 °C captured by MosaicX under oil immersion microscopy. Focused cross-section of thin-walled and thick-walled bio-char extracted from the yellow dotted region of (k) 850 and (l) 950 °C sample.

that cellulose-dominant samples produce bio-oil-rich products; hemicellulose-dominant biomass yields bio-gas products whilst lignin-dominant samples are more inclined towards producing bio-char-rich products.

Previous studies compared and investigated the formation of thin- and thick-walled bio-char and their properties at varying cellulose, hemicellulose and lignin compositions [3,28]. The published work established the increase in secondary walls increases the percentage of thick-walled bio-char but reduces the char reactivity during thermal conversion. This current work is an extension where: (1) microscopic graphical illustrations of the transformation of individual lignocellulosic components, (2) the influence of pyrolytic conditions on the behaviours of lignocellulose, as well as (3) the characteristics of the final bio-char products are investigated to facilitate categorisation of biomass for targeted engineering applications.

3.2.2. *Reflectance and dimensions via oil immersion microscopy*

Bio-char samples are bounded for observation under the oil immersion microscope as illustrated in Fig. 3 to study the evolution of biomass structures after pyrolysis. The comparison between fresh and pyrolysed samples is important to understand the reactions of individual cells and the structural change of lignocellulosic components in primary and secondary cell walls during pyrolysis. The exterior parameters such as total area of sample cross-section, average diameter of vascular bundle and mean pixel intensity of pyrolysed samples in greyscale were evaluated via the image analysis tool, ImageJ. The calculated results along with the bio-char yields are tabulated in Table 2.

The average area of bamboo culms, diameter of vascular bundles and bio-char yields reduced after pyrolysis and appeared to decrease gradually as pyrolysis temperature increased, as tabulated in Table 2. The size reduction in macroscopic view is attributed to sample shrinkage during the thermal treatment as the lignocellulosic components in the cell walls decomposed and were released as volatiles. Similarly, the decrease of bio-char yields at higher temperatures is associated with the greater decomposition of organic components, promoting the release of volatile materials at elevated temperatures. The magnitude of decomposition is associated with the thickness of cell walls as biomass experiences both heat transfer and chemical kinetic change during pyrolysis [29]. In microscopic view, the uniform heat transfer across thin-walled parenchyma cells facilitates cellulose and hemicellulose decomposition and reduces the residence time of volatiles, which subsequently limits the secondary conversion of tar. As described in section 3.2.1, cellulose polymer chains undergo successive molecular and radical reactions yielding 80% of condensable volatile components such as hydroxyacetaldehyde (HAA), formaldehyde and acetaldehyde; whilst hemicellulose mainly yields gaseous products from dehydration, dehydrogenation and demethylation. It is apparent from Fig. 3 that most of the cellulose- and hemicellulose-containing parenchymatous cells and unlignified interior of vascular bundles have devolatilised and are generally not visible under the microscope. Nonetheless, minor fractions of parenchymatous cells are observed to have formed thin-walled bio-chars as illustrated in Fig. 3k and l, whilst lignified fibre sheath formed thick-walled bio-chars, thus validating that both cellulose and hemicellulose are contributing to the formation of bio-char samples despite yielding mainly bio-oil and bio-gas products during pyrolysis.

On the contrary, heat transfer in thick-walled sclerenchyma cells is not spatially uniform where pyrolysis reaction takes place starting from the surface, resulting in a yet-to-react core surrounded by bio-char layers. As the volatiles escape and diffuse through the bio-char layers, the chemical kinetic changes outpace heat transfer within the cell walls and secondary pyrolysis reactions occur. The cracking and repolymerisation of tar resulted in a greater magnitude of sample shrinkage and is more pronounced in samples pyrolysed at higher temperatures as tabulated in Table 2. Meanwhile, lignin as the glueing matrix for cellulose microfibrils, particularly in sclerenchyma, exhibits intrinsic nature of being thermally stable and is more resilient to decomposition [17]. Thus, the formation of thick-walled bio-char structures from secondary cell walls could be attributed to this unique characteristic of lignin.

The degree of repolymerisation of bio-char appeared to be proportional to the reaction temperature as illustrated across Fig. 3a–j. The sizes and distribution of voids remaining after devolatilisation in sample pyrolysed at higher temperatures are relatively bigger and more regular as compared to that of lower temperatures. In addition, the sintering effect of bio-char particles increases at higher temperatures, thus increasing the sample density and crystallinity of bio-char. The pixel intensity of bio-char samples captured under oil immersion microscope is primarily affected by the reflectance, which is directly related to the crystallinity and arrangements of carbon structures in bio-char [30]. As pyrolysis temperature increases, the bio-char samples exhibit a higher reflectance but experience a gradual drop at 850 °C, followed by a peak at 950 °C. Such observation trend will be combined with crystallographic and graphitisation parameters as well as pore structures of bio-char that are further characterised via XRD, Raman spectroscopy and BET, respectively, to understand and validate the influence of pyrolytic temperature on plant cell wall structures and their resultant bio-char characteristics.

3.2.3. *Carbon lattice and crystallinity*

The 2θ angle peaks at 16 and 22° observed in the XRD spectra reveal

Table 2
Exterior parameters of biomass and bio-char calculated via image analysis.

Sample	Area of sample cross-section (mm^2)	Average area of a single vascular bundle (μm)	Mean pixel intensity in greyscale	Bio-char yield (wt %)
Fresh	2.10	7039.33	–	–
550	1.75	6447.39	49.43	29.52
650	1.80	4807.04	69.84	26.22
750	1.47	4711.70	72.88	26.23
850	1.31	4556.22	50.03	25.01
950	0.58	3633.18	81.37	24.29

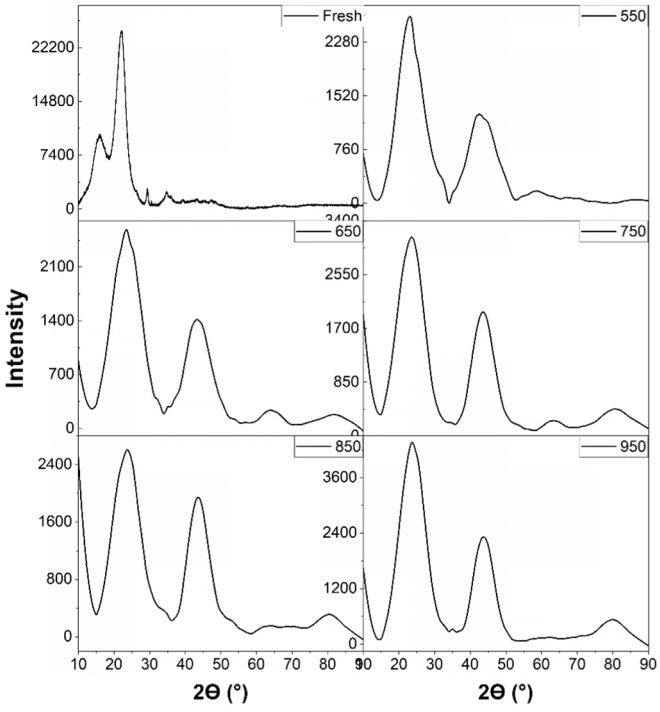

Fig. 4. XRD spectra of fresh bamboo sample and bio-char produced at pyrolysis temperature of 550 to 950 °C.

that the crystallographic planes of cellulose in the raw sample were lost after pyrolysis as illustrated in Fig. 4. All of the bio-char samples produced at pyrolysis temperatures above 550 °C exhibit similar diffraction patterns with two broad peaks at approximately 23° and 44° corresponding to the graphitic planes of (0 0 2) and (1 0 0), respectively. The (0 0 2) peak suggests the presence of graphite-like structures and represents the inter-reticular distance of graphitic basal planes of crystallites; whilst the (1 0 0) peak is attributed to the graphite-like atomic order in single plane and reflects the degree of aromatic ring condensation. The asymmetry (0 0 2) peak with a γ band appearing at 20° is associated with the presence of saturated structures such as functional groups, aliphatic side chains and/or hydrocarbons that are attached to the edges of crystallites.

The diffraction peaks of (1 0 0) sharpen and the intensities of the (0 0 2) peaks increase as the pyrolysis temperature increases from 550 to 750 °C, indicating a higher-ordered carbon structure was formed. However, the intensity of (0 0 2) peak experiences a decrease at 850 °C prior to a sharp increase at 950 °C. The noticeable reduction in the intensity of the 850 °C bio-char could be attributed to the transition of an amorphous bio-char into a turbostratic bio-char where the microcrytallites have the structure ordering of that in between amorphous and crystalline graphite phase at a higher synthesis temperature [31,32]. As the pyrolytic temperature increased to 950 °C, the crystalline graphitic structures with enhanced crystallinity are formed, thus producing an XRD spectrum with higher intensity. Pyrolysis temperature of 850 °C could be the transition temperature from turbostratic to crystalline bio-char for the selected bamboo biomass. This statement agrees well with the bio-char reflectance trend as analysed by ImageJ and is also further validated by Raman and BET analysis in the following sections.

Carbon lattice parameters such as interlayer spacing (d_{002} and d_{100}), crystallite height (L_c) and crystallite diameter (L_a) calculated using Eqs. (5)–(7) are tabulated in Table 3. The decrease in interlayer spacing is associated with the abscission of non-aromatic structures such as aliphatic side chains and oxygen-containing functional groups at higher pyrolysis temperatures. The reduction of non-aromatics thus facilitates the reconstruction of crystalline structure in the longitudinal direction (increasing L_c). Similarly, with the decrease of oxygen-containing functional groups with increasing temperatures, more active sites are available for aromatic rings to condense, thus gradually increasing the crystallite size (L_a). In addition, the increased ratio of L_a/L_c across the temperature range of 550–950 °C indicated that the growth of crystallite units in the transverse direction is greater than that in the longitudinal direction. The aromatic structural system becomes larger and the molecular arrangements are enhanced to be more regular, which subsequently results in a denser bio-char structure.

3.2.4. Graphitisation and defects

Fig. 5 illustrates the Raman spectra of bio-char produced across the pyrolysis temperatures of 550–950 °C where typical D and G bands at approximate 1350 cm^{-1} and 1590 cm^{-1}, respectively, are observed. Both the D and G bands are evidence of polyaromatic hydrocarbons and graphitic materials. The D band reveals the disordered graphite rings whilst the G band represents the vibrations of sp^2 carbon atoms in the graphitic materials. The ratio between the D and G band area, I_D/I_G, is a parameter widely used to define the graphitisation ratio and crystalline structure of a material. In general, the increase in pyrolysis temperature

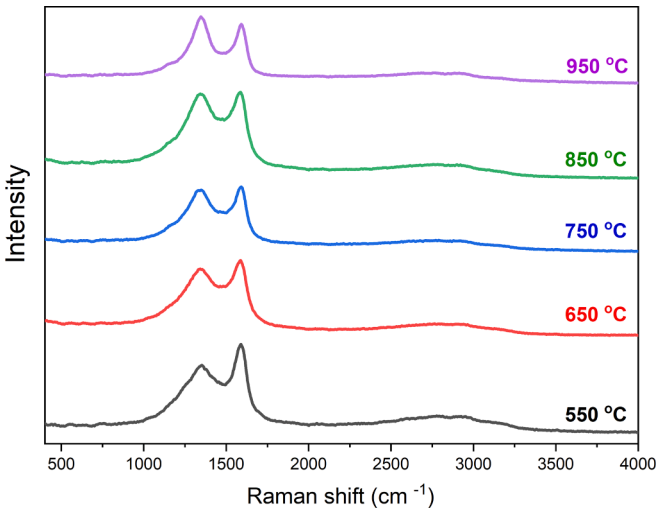

Fig. 5. Raman spectra of bio-char produced at pyrolysis temperature of 550 to 950 °C.

leads to a decrease in I_D/I_G as graphitic structures are expected to grow, revealing the crystalline orders. However, as indicated in Section 3.2.3 regarding the transition of amorphous to crystalline bio-char structures, Raman spectroscopy has also recorded the pyrolysis of biomass that took place in two different regimes, namely initial carbonisation phase and graphitisation regime, where the I_D/I_G ratios increase with the increase in pyrolysis temperature at the initial carbonisation phase but reduce at the graphitisation regime as tabulated in Table 4. The rise in I_D/I_G ratio indicates heteroatoms are released from the precursors and this phenomena is typically observed in amorphous carbon materials existing in the temperate range before the occurrence of turbostratic carbon structures [33]. The increasing pyrolysis temperature gives rise to the condensation reactions of aromatic ring systems and allows the formation of benzene-fused rings [34]. As the reaction proceeds into the graphitisation regime, continuous condensation reaction results in the broadening of aromatic systems, which agrees with the XRD results, and a sharp drop in the I_D/I_G ratio was observed. The decrease in I_D/I_G value at 950 °C suggests the increasing order of sp^2 bonded graphitic domains occurred and reiterates 850 °C as the transitional turbostratic phase in between amorphous and crystalline bio-char.

3.2.5. Pore structures and surface structures

As the morphology of char structures evolves, sample shrinkage is often accompanied by porosity gain during pyrolysis. The pore

Table 4
Band details and I_D/I_G ratio of bio-char produced at different temperatures.

Temperature (°C)	D-band area (×10^5)	G-band area (×10^5)	I_D/I_G
550	8.15	2.47	3.30
650	8.11	1.99	4.08
750	6.49	1.55	4.18
850	9.85	2.15	4.57
950	4.58	1.57	2.91

Table 3
Carbon lattice parameters of bio-char produced at pyrolysis temperature of 550–950 °C.

Temperature (°C)	$2\Theta_{002}$ (°)	$2\Theta_{100}$ (°)	β_{002} (°)	β_{100} (°)	d_{002}(Å)	d_{100}(Å)	L_c (Å)	L_a(Å)	L_a/L_c
550	23.08	42.57	8.10	9.00	3.85	2.12	9.90	19.38	1.96
650	23.45	43.26	9.60	8.80	3.79	2.09	8.36	19.85	2.38
750	23.55	43.59	9.10	7.60	3.77	2.07	8.82	23.02	2.61
850	23.71	43.59	9.00	7.20	3.75	2.07	8.92	24.29	2.68
950	23.66	43.71	8.60	7.00	3.75	2.07	9.33	25.00	2.68

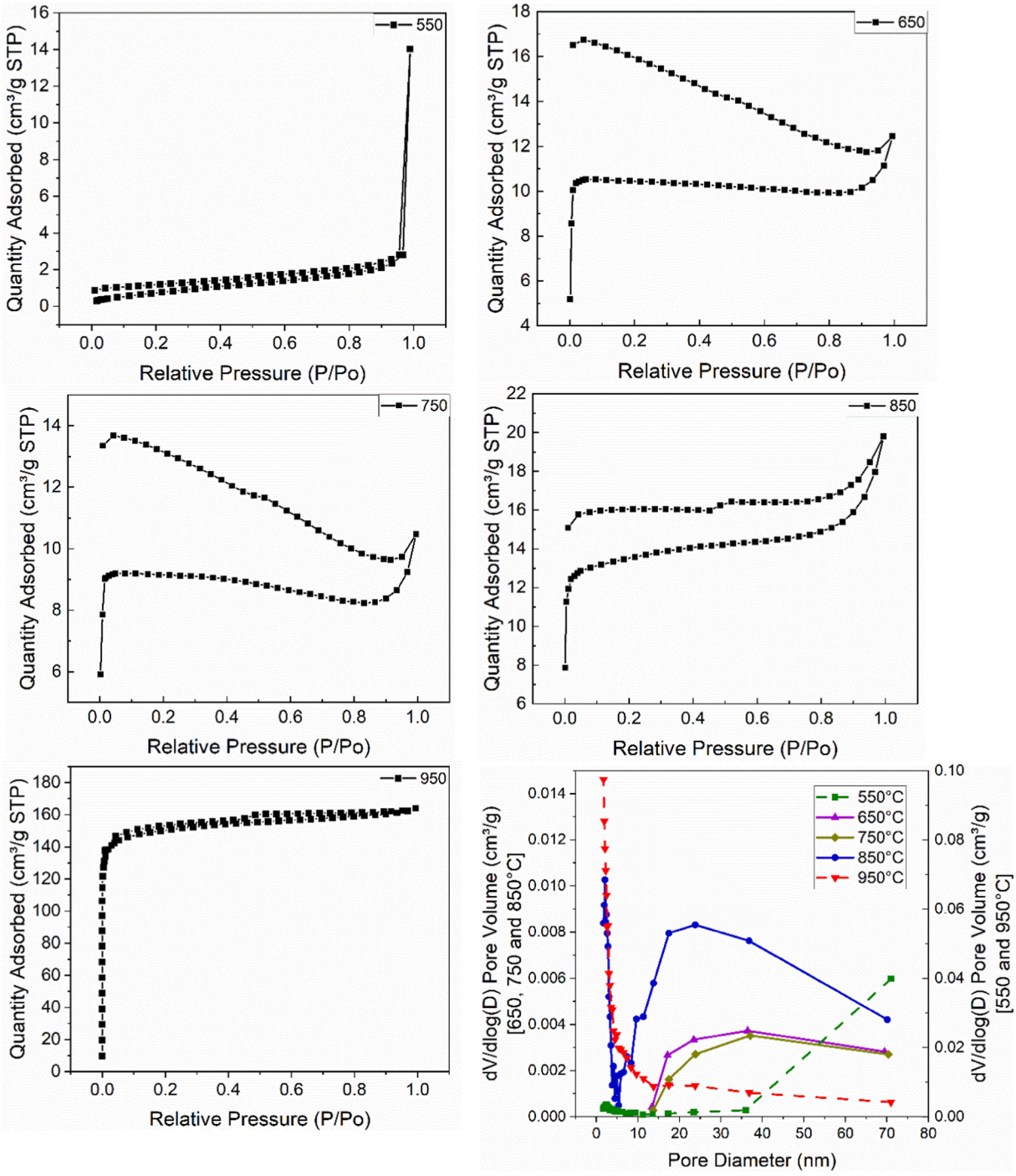

Fig. 6. Individual adsorption–desorption isotherms of bio-char samples produced at different pyrolysis temperatures and pore size distribution of all five bio-char samples.

structures of bio-char are analysed based on the specific surface area, pore volume and pore size distribution performed by the nitrogen adsorption–desorption of bio-char. The isotherms produced at different pyrolysis temperatures as illustrated in Fig. 6 are identified as type IV isotherms according to the International Union of Pure and Applied Chemistry (IUPAC) classification [35] arising from bio-chars with micropore (<2 nm), mesopore (2–50 nm) and macropore (>50 nm) structures.

All bio-char samples produced from 550–950 °C exhibit type IV isotherms. The capillary condensation associated with the interactions between gas molecules and pore surfaces results in a diverging desorption path, thus forming a hysteresis loop and revealing the specific pore geometry and connectivity in the bio-char samples. Samples produced at 650, 750 and 850 °C exhibit the H2 type hysteresis loop, indicating a disordered distribution of pore size and the bottleneck constrictions in pores. The near-complete hysteresis loop in the samples is associated with the complex internal pore network structure and the incomplete desorption of nitrogen during analysis [36]. The irreversible uptake of adsorbate molecules and tar components which subsequently condensed within the pores interfered with the adsorption–desorption process, thus leading to incomplete isotherms. Conversely, bio-char produced at 950 °C features a type IV isotherm with a H4 hysteresis loop, indicating high degree of microporosity with narrow slit-like pore formations in the sample. Similarly, 550 °C bio-char also exhibits a type IV isotherm with

H4 hysteresis loop but the adsorption capacity of 550 °C bio-char is exceedingly lower than that of 950 °C. Note that the pores of 550 °C bio-char as illustrated in Fig. 6 consist mainly of macropores, thus reflecting in limited N_2 adsorption of the bio-char sample as compared to 950 °C bio-char with high percentage of micropores.

The pore structure parameters of bamboo bio-char are tabulated in Table 5. The transformation of biomass cell structures is also observed to occur via three bio-char stages, namely amorphous, turbostratic and crystalline. At a lower pyrolysis temperature of 550 °C, volatiles are mainly released from the thermal degradation of cellulose and hemicellulose. As pyrolysis progresses to a higher temperature of 850 °C, the continuous degradation of lignin occurs and 2D structures of fused rings are formed. It is noteworthy that the total pore volume and surface area increased, indicating the mesopore structures are gradually replaced by the micropore structures in the turbostratic bio-char [37]. As the pyrolytic temperature increases to 950 °C, the bio-char structures are transformed from turbostratic to crystalline structures as 2D fused rings are converted into graphitic microcrystalline structures resulting in a larger magnitude of increase in surface area. The pore size distribution in Fig. 6 illustrates and suggests the occurrence of turbostratic bio-char at 850 °C as it exhibits both the characteristics of amorphous (550–750 °C) and crystalline (950 °C) bio-char. Such result trend is also in accordance with the discussions of image analysis, XRD and Raman spectra.

The increase in micropore area and volume as pyrolysis temperature increases, particularly 950 °C bio-char (approximately 91% of total pore area and 60% of total pore volume), is mainly attributed to the decomposition of all three lignocellulosic components, i.e. cellulose, hemicellulose and lignin resulting in the release of volatiles, especially in the degradation of benzene-ring compounds in lignin. Similarly, the fusion of rings and the growth of graphite microcrystals during pyrolysis results in cracks in the overall carbon structure thus reflected in the increase of micropore volume. The pyrolysis temperature clearly impacts the surface area and pore size distribution in bio-char, thus enabling control during future biomass processing.

3.3. Future prospects and applications

Despite extensive studies have been performed on biomass processing, behaviours of the fundamental lignocellulosic components during thermal conversion are yet to be comprehensively described. This study investigates the anatomy and biological functions of different cell types in bamboo to examine the structural evolution of primary and secondary plant cell walls during pyrolysis. The composition of lignocellulosic components highly influences the resultant bio-char structure and properties, thus, it is crucial to understand its decomposition behaviours and predict the suitable biomass feedstock for targeted engineering applications, i.e. energy derivation and/or material engineering. The interaction between varying pyrolysis temperatures and resultant bio-char properties are summarised in Fig. 7. The graphitic illustration provides insight into an effective biomass selection for different applications.

Amongst various conversion processes, pyrolysis is one of the most established methods for biomass processing and is considered as the first step of many other thermal conversion processes including combustion and gasification for energy derivation [17]. Previous studies concluded that samples with higher percentages of cellulose and hemicellulose are prone to devolatilise [22] and thus are more desired for better production yield, as well as producing bio-char with lower crystallinity to avoid pipeline clogging or other operational challenges during renewable fuels harvesting. Current industrial trends agree well with the aforementioned conclusion where the top 5 biomass processed globally for biofuels derivation [38,39] including corn, soybean, sugarcane, wheat and canola contain higher primary wall constituents than lignified components, i.e., cellulose at 22–67%, hemicellulose at 16–50% and lignin at 11–27% [40-44].

On the contrary, feedstocks with lignified secondary walls, typically woody and coniferous biomass are desirable in kraft pulping and material engineering [45]. Recent studies reported successful derivation of various nanomaterials from biomass where graphene was produced from pyrolysis of camphor sample [46] and populus wood [47], as well as graphene aerogels from hydrothermal treatment of Longjing tea waste [48]. The general population of such samples contain relatively higher lignified secondary components, i.e., cellulose at 30–49%, hemicellulose 7–27% and lignin at 18–45% [40,41,49] than other biomass. This reiterates the potential of lignified biomass that produces dense bio-char structures as a carbon precursor to replace natural graphite in materials engineering.

Amongst different bio-char structures, amorphous bio-char contains porous surfaces that are suitable for various functionalisation, including doping and surface recombination. Amorphous bio-char bearing sulfonic group is a typical alternative solid acidic material that can be easily separated from reaction mixtures via simple filtration or centrifugation; and is an alternative to improve the efficiency of catalysation processes by replacing liquid catalytic acids [50]. Moreover, amorphous bio-char facilitates surface recombination for nanoparticle loading or alloying. Enhancement in the reactivity of the supported nanoparticles during photocatalysis reactions has been reported in hybrid structures of bio-char with boron, palladium or titanium dioxide nanoparticles [51]. Conversely, crystalline bio-chars are comparatively more stable than the reactive amorphous bio-chars and could bypass the modification procedures prior to the conversion into advanced materials [52]. Crystalline bio-char exhibit various properties similar to that of natural graphite and hence has great potential as a substitute to reduce the dependency on non-renewable graphitic feedstocks for graphene-based nanomaterials production. Whilst the use of biomass feedstock is commonly acknowledged as a sustainable alternative, the implicit impacts that originate from improper biomass processing are often debatable. Therefore, the comprehensive understanding of biomass intrinsic properties, particularly the lignocellulosic components, is essential to provide a more effective and efficient selection to maximise the full potential of each biomass category, as well as to accelerate carbon–neutral processing.

Table 5
Pore structure parameters of bio-char produced at 550–950 °C.

Temperature (°C)	Surface area (m^2/g)	Total pore volume (mm^3/g)	Average pore size (nm)
550	17.06	14.46	4.19
650	35.87	2.76	41.00
750	31.43	2.68	41.99
850	46.78	9.48	10.90
950	533.36	35.58	3.42

4. Conclusions

This study investigated the pyrolytic behaviours of lignocellulose and provided insights into the correlation between individual cells and pyrolytic product distribution, as well as properties of resultant bio-char that are useful for efficient biomass selection in energy derivation and material engineering sectors. Primary cell walls mainly consist of cellulose that devolatilise and are not visible under the microscope post pyrolysis are highly stained by fast green solution. Conversely, safranin O solution has higher affinity to lignified secondary cell walls that decompose into bio-char. Cells evolve into amorphous, turbostratic and crystalline bio-char as pyrolytic temperature increases. Crystalline bio-chars generally have enhanced crystallinity, reflectance, surface area and pore volume.

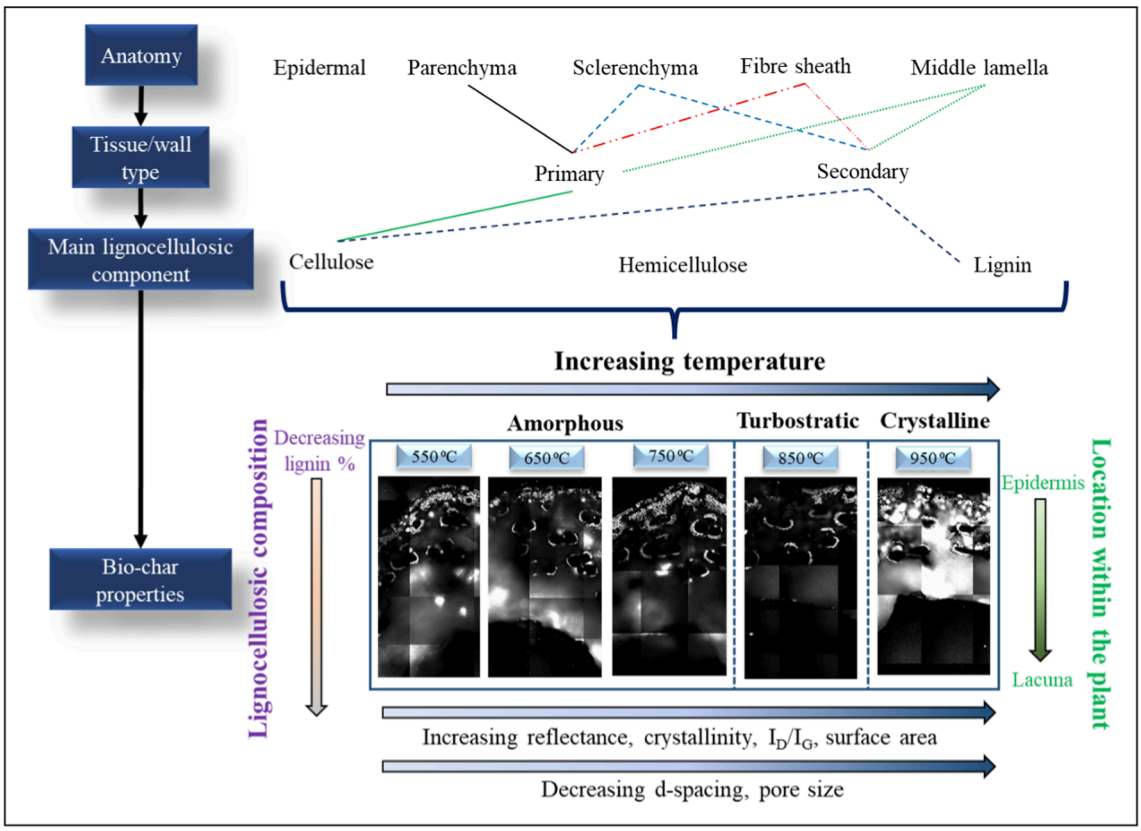

Fig. 7. Summary of cell types, lignocellulosic components and the influence of pyrolytic conditions on resultant bio-char properties.

CRediT authorship contribution statement

Yoong Xin Pang: Writing – original draft, Visualization, Formal analysis, Methodology, Investigation. **Nusrat Sharmin:** Validation, Writing – review & editing. **Tao Wu:** Validation, Resources, Supervision, Writing – review & editing. **Cheng Heng Pang:** Conceptualization, Validation, Resources, Supervision, Project administration, Writing – review & editing.

Declaration of Competing Interest

The authors declare that they have no known competing financial interests or personal relationships that could have appeared to influence the work reported in this paper.

Data availability

Data will be made available on request.

Acknowledgements

The authors gratefully express gratitude to all parties who have contributed towards the success of this project, both financially and technically, especially the S&T Innovation 2025 Major Special Programme [Grant number 2018B10022] and the Ningbo Commonweal Programme [Grant number 2022S122] funded by the Ningbo Science and Technology Bureau, China, as well as the UNNC FoSE Faculty Inspiration Grant, China. The authors would like to acknowledge the support from the Ningbo Municipal Key Laboratory on Clean Energy Conversion Technologies [2014A22010] as well as the Zhejiang Provincial Key Laboratory for Carbonaceous Wastes Processing and Process Intensification Research funded by the Zhejiang Provincial Department of Science and Technology [2020E10018].

References

[1] Zong P, et al. Pyrolysis behavior and product distributions of biomass six group components: starch, cellulose, hemicellulose, lignin, protein and oil. Energ Conver Manage 2020;216:112777.
[2] Tursi A. A review on biomass: importance, chemistry, classification, and conversion. Biofuel Res J 2019;22:962–79.
[3] Pang CH, et al. Relationship between thermal behaviour of lignocellulosic components and properties of biomass. Bioresour Technol 2014;172:312–20.
[4] Cosgrove DJ. Re-constructing our models of cellulose and primary cell wall assembly. Curr Opin Plant Biol 2014;22:122–31.
[5] Sakamoto S, et al. Complete substitution of a secondary cell wall with a primary cell wall in Arabidopsis. Nat Plants 2018;4(10):777–83.
[6] Yan Y, et al. Synthesis of graphene oxide and graphene quantum dots from miscanthus via ultrasound-assisted mechano-chemical cracking method. Ultrason Sonochem 2021;73:105519.
[7] Liu H, et al. A hybrid kinetic and optimization approach for biomass pyrolysis: the hybrid scheme of the isoconversional methods, DAEM, and a parallel-reaction mechanism. Energ Conver Manage 2020;208:112531.
[8] AccessScience E. Potential uses of biochar; 2016.
[9] Rodriguez-Narvaez OM, et al. Biochar-supported nanomaterials for environmental applications. J Ind Eng Chem 2019;78:21–33.
[10] Huang YF, et al. Pyrolysis kinetics of biomass from product information. Appl Energy 2013;110:1–8.
[11] Weng J, et al. Pyrolysis study of poplar biomass by tunable synchrotron vacuum ultraviolet photoionization mass spectrometry. Proc Combust Inst 2013; 34(2): 2347–54.
[12] Ranzi E, et al. Kinetic modeling of the thermal degradation and combustion of biomass. Chem Eng Sci 2014;110:2–12.
[13] Simone M, et al. Evaluation of global biomass devolatilization kinetics in a drop tube reactor with CFD aided experiments. Fuel 2009;88(10):1818–27.
[14] Brown AL, et al. Design and characterization of an entrained flow reactor for the study of biomass pyrolysis chemistry at high heating rates. Energy Fuel 2001;15(5): 1276–85.
[15] Lozano EM, Pedersen TH, Rosendahl LA. Modeling of thermochemically liquefied biomass products and heat of formation for process energy assessment. Appl Energy 2019;254:113654.
[16] Jemaa M, et al. Simulation of biofuel production via fast pyrolysis of palm oil residues. Fuel 2015;159.
[17] Pang YX, et al. The influence of lignocellulose on biomass pyrolysis product distribution and economics via steady state process simulation. J Anal Appl Pyrol 2021;158:104968.

[18] Adeeyo O, Oresegun OM, Oladimeji TE. Compositional analysis of lignocellulosic materials: evaluation of an economically viable method suitable for woody and non-woody biomass. Am J Eng Res (AJER) 2015;4(4):14–9.
[19] Boral P, Varma AK, Maity S. X-ray diffraction studies of some structurally modified Indian coals and their correlation with petrographic parameters. Curr Sci 2015: 384–94.
[20] Okolo GN, et al. Chemical–structural properties of South African bituminous coals: insights from wide angle XRD–carbon fraction analysis, ATR–FTIR, solid state 13C NMR, and HRTEM techniques. Fuel 2015;158:779–92.
[21] Bar-On Y, Phillips R, Milo R. The biomass distribution on Earth. In: Proceedings of the national academy of sciences, vol. 115; 2018. p. 201711842.
[22] Pang YX, et al. Analysis of environmental impacts and energy derivation potential of biomass pyrolysis via Piper diagram. J Anal Appl Pyrol 2021;154:104995.
[23] The State Council of The People's Republic of China. China has over 6m hectares of bamboo forests, in Xinhua; 2021.
[24] Hsiung W. Bamboo in China: new prospects for an ancient resource. Unasylva Int J Forest Forest Ind 1987.
[25] Alqus R, Eichhorn SJ, Bryce RA. Molecular dynamics of cellulose amphiphilicity at the graphene-water interface. Biomacromolecules 2015;16(6):1771–83.
[26] Mazeau K, Rivet A. Wetting the (110) and (100) surfaces of I?? Cellulose studied by molecular dynamics. Biomacromolecules 2008;9:1352–4.
[27] Yamane C, et al. Two different surface properties of regenerated cellulose due to structural anisotropy. Polym J 2006;38:819–26.
[28] Pang CH, Lester E, Wu T. Influence of lignocellulose and plant cell walls on biomass char morphology and combustion reactivity. Biomass Bioenergy 2018;119:480–91.
[29] Babu BV, Chaurasia AS. Heat transfer and kinetics in the pyrolysis of shrinking biomass particle. Chem Eng Sci 2004;59(10):1999–2012.
[30] Avansi W, et al. Role of crystallinity on the optical properties of Na2V6O16·3H2O nanowires. J Alloy Compd 2018;731:1119–24.
[31] Acauan LH, Kaiser AL, Wardle BL. Direct synthesis of carbon nanomaterials via surface activation of bulk copper. Carbon 2021;177:1–10.
[32] Schimmelpfennig S, Glaser B. One step forward toward characterization: some important material properties to distinguish biochars. J Environ Qual 2011;41: 1001–13.
[33] Pusceddu E, et al. Chemical-physical analysis and exfoliation of biochar-carbon matter: from agriculture soil improver to starting material for advanced nanotechnologies. Mater Res Exp 2019;6(11):115612.
[34] Azargohar R, et al. Effects of temperature on the physicochemical characteristics of fast pyrolysis bio-chars derived from Canadian waste biomass. Fuel 2014;125: 90–100.
[35] Sing KS. Reporting physisorption data for gas/solid systems with special reference to the determination of surface area and porosity (Recommendations 1984). Pure Appl Chem 1985;57(4):603–19.
[36] Ma Z, et al. Gasification of rice husk in a downdraft gasifier: the effect of equivalence ratio on the gasification performance, properties, and utilization analysis of byproducts of char and tar. BioResources 2015;10(2):2888–902.
[37] Zhang Y, et al. Comparison of the physicochemical characteristics of bio-char pyrolyzed from moso bamboo and rice husk with different pyrolysis temperatures. BioResources 2017;12(3):4652–69.
[38] National Renewable Energy Laboratory. Biomass Energy Basics; 2023. https://www.nrel.gov/research/re-biomass.html.
[39] Office of Energy Efficiency & Renewable Energy. Biofuel Basics. n.d. https://www.energy.gov/eere/bioenergy/biofuel-basics.
[40] Kumar S, Shukla S. A review on recent gasification methods for biomethane gas production. Int J Energy Eng 2016;6(1A):32–43.
[41] Jahirul MI, et al. Biofuels production through biomass pyrolysis —a technological review. Energies 2012;5:4952–5001.
[42] Wang M, et al. To distinguish the primary characteristics of agro-waste biomass by the principal component analysis: an investigation in East China. Waste Manag 2019;90:100–20.
[43] Baruah J, et al. Recent trends in the pretreatment of lignocellulosic biomass for value-added products. Front Energy Res 2018:6.
[44] Muktham R, et al. A review on 1st and 2nd generation bioethanol production-recent progress. J Sust Bioenergy Syst 2016;6:72–92.
[45] Chen H. 3 - Lignocellulose biorefinery feedstock engineering. In: Chen H, editor. Lignocellulose biorefinery engineering. Woodhead Publishing; 2015. p. 37–86.
[46] Shams SS, et al. Synthesis of graphene from biomass: a green chemistry approach. Mater Lett 2015;161:476–9.
[47] Ekhlasi L, et al. Populus wood biomass-derived graphene for high CO2 capture at atmospheric pressure and estimated cost of production. Process Saf Environ Prot 2018;113:97–108.
[48] Li N, et al. Bioinspired green tea waste/graphene aerogel for solar-enhanced uranium extraction from seawater. Desalination 2023;545:116153.
[49] Demirbas A. Effects of temperature and particle size on bio-char yield from pyrolysis of agricultural residues. J Anal Appl Pyrol 2004;72(2):243–8.
[50] Nakajima K, Hara M. Amorphous carbon with SO3H groups as a solid brønsted acid catalyst. ACS Catal 2012;2:1296–304.
[51] Liu W-J, Jiang H, Yu H-Q. Development of biochar-based functional materials: toward a sustainable platform carbon material. Chem Rev 2015;115(22): 12251–85.
[52] Pal A, Sk MP, Chattopadhyay A. Recent advances in crystalline carbon dots for superior application potential. Mater Adv 2020;1(4):525–53.